Graphic Displays of Gravitational Initial Data

JEFFREY M. BOWEN

Bucknell University, Lewisburg, Pennsylvania 17837

The use of perspective graphic displays that facilitate the understanding of numerical solutions is discussed. As a particular example from my own field, successive overrelaxation is used to solve a boundary value problem for gravitational initial data describing a moving black hole. Two techniques of data enhancement are described, and several graphic displays are presented which vividly reveal the detailed radial and angular dependence of the gravitational conformal factor.

1. INTRODUCTION

In recent years, significant progress has been made in developing a procedure for solving problems in gravitational dynamics. The basic program, as described by Smarr and York [1–3], requires one to choose a spacelike hypersurface, solve a set of initial value constraints on this surface, and then evolve this initial data as a Cauchy problem. Misner [4] and Lindquist [5] have solved analytically the initial value constraints for the problem of many stationary uncharged or charged black holes. Because their solutions dealt with initially stationary black holes, the momentum constraint was satisfied by the trivial zero solution. An analytic solution of the full initial value problem does not presently exist for the case of non-zero initial momentum. For this more general case, numerical techniques offer the best hope for providing initial data that can be used in future evolution calculations. However, interpretation of numerical results is often difficult. An especially useful tool for understanding such results is a perspective graphic display. Extending the work of York and Piran [6], this paper describes an independent numerical solution of an important initial value problem—that of a single moving black hole—and presents graphic displays of some of the results.

Following this introduction, we state the boundary value problem to be solved and discuss the numerical methods used in the solution. Section 3 describes two techniques of data enhancement, the graphics package, and the conversion of spherical data to the more convenient Cartesian system. In Section 4, we present and discuss the graphic displays. Finally, conclusions and applications to other problems are given in Section 5.

2. Numerical Solution of the Boundary Value Problem

The physical problem to be addressed here is that of specifying at a given instant certain gravitational data that describe a single moving black hole. Starting from the vacuum initial value equations of general relativity, Bowen and York [7] present an explicit closed-form solution of one of these equations, the momentum constraint. They then go on to describe a boundary value formulation that can determine a unique solution of the other initial value equation, the Hamiltonian constraint. That problem is

$$\nabla^2 \psi = -\frac{1}{8} H \psi^{-7} \qquad \text{for} \quad r \geqslant a \qquad (1)$$

$$\frac{\partial \psi}{\partial r} + \frac{1}{2a} \psi = 0 \qquad \text{for} \quad r = a \qquad (2)$$

$$\psi > 0, \qquad \lim_{r \to \infty} \psi = 1, \qquad (3)$$

where ∇^2 is the three-dimensional flat-space Laplacian operator, ψ is the gravitational conformal factor, H is the source factor containing the momentum of the hole, r is the usual radial coordinate, and a is a constant proportional to the size of the momentum source. The inner boundary condition (2) is related to (in fact is derivable from) a special symmetry property of the conformal factor. I have elsewhere shown that, in the final physical geometry for this problem, a simple spherical inversion map is an isometry [8]. If we take a as the radius of inversion, this symmetry property can be written

$$\psi(r, \Theta, \phi) = \frac{a}{r} \psi \left(\frac{a^2}{r}, \Theta, \phi \right) \qquad (4)$$

from which (2) follows by differentiation. Condition (4) will be used in Section 3 to generate data inside $r = a$.

To proceed with the numerical solution of the boundary value problem (1)–(3), we must specify H. Using the solution of the momentum constraint presented by Bowen and York, we find

$$H = \frac{9}{2} \frac{P^2}{r^4} \left[\left(1 + \frac{a^2}{r^2} \right)^2 + 2 \cos^2 \Theta \left(1 - 4 \frac{a^2}{r^2} + \frac{a^4}{r^4} \right) \right], \qquad (5)$$

where P is the magnitude of the momentum of the moving hole, and Θ is measured from the direction of motion. It is also useful to study the numerical solution for the "model H" offered by Bowen and York,

$$H_{\text{model}} = 6 \frac{P^2}{r^4} \left(1 - \frac{a^2}{r^2} \right)^2, \qquad (6)$$

since this form admits an exact solution

$$\psi_{\text{model}} = \left(1 + \frac{2E}{r} + \frac{6a^2}{r^2} + \frac{2a^2E}{r^3} + \frac{a^4}{r^4}\right)^{1/4}, \tag{7}$$

where the total energy is given in this case by $E = (P^2 + 4a^2)^{1/2}$. Although there is no angular dependence in H_{model}, it has proven valuable in testing the two-dimensional iteration scheme. Plots of H and H_{model} appear in Fig. 1.

Now that we have specified the source function H in the scale Eq. (1), we address boundary conditions (2) and (3). Although the inner condition at $r = a$ presents no problem for a numerical solution, we cannot extend the radius indefinitely to apply the outer condition, $\lim_{r \to \infty} \psi = 1$. Since we expect $\psi = 1 + E/2r + O(1/r^2)$, we form $\partial\psi/\partial r = -E/2r^2 + O(1/r^3)$. Then ignoring $O(1/r^3)$, we find

$$\frac{\partial\psi}{\partial r} + \frac{1}{R}(\psi - 1) = 0 \qquad \text{for} \quad r = R, \tag{8}$$

where R is an artificial outer boundary such that $R \gg a$.

We may reduce the region of integration by a factor of four if we exploit the angular symmetry of H and ψ. Since both depend on angle only through $\cos^2\Theta$, we obtain the boundary conditions

$$\frac{\partial\psi}{\partial\Theta} = 0 \qquad \text{at } \Theta = 0 \text{ and } \Theta = \pi/2.$$
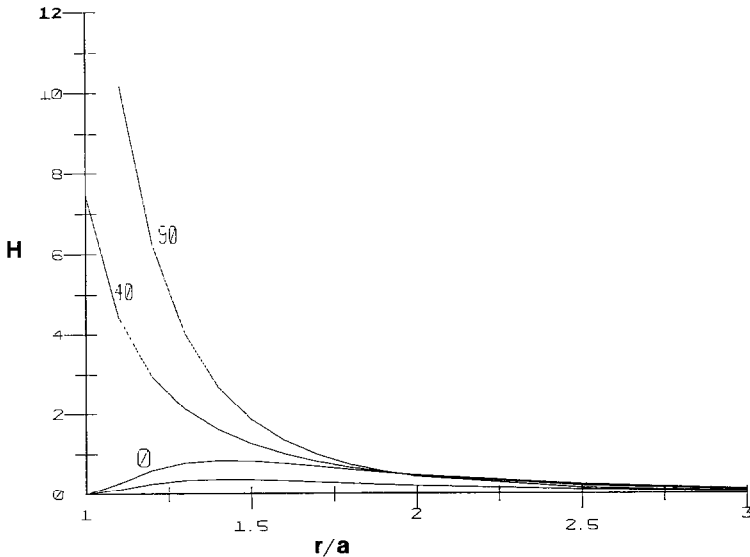

FIG. 1.   The source functions H and H_{model}, given by Eqs. (5) and (6). Labeled curves are of H, with the angle given in degrees. The unlabeled curve at the bottom is H_{model}. Note that H for $0°$ is $\frac{9}{4}H_{\text{model}}$. The dimensions of H are a^{-2}, and $(P/a) = 1$ for this plot.

Finally we note that the entire problem is azimuthally symmetric and thus the entire dimension associated with ϕ may be ignored by considering only the slice $\phi = 0$. Thus our complete value problem, appropriate for a finite two-dimensional region, is

$$\nabla^2 \psi = -\frac{1}{8} H \psi^{-7} \qquad \text{for } a \leqslant r \leqslant R \text{ and } 0 \leqslant \Theta \leqslant \pi/2 \qquad (9)$$

$$\frac{\partial \psi}{\partial \Theta} = 0 \qquad \text{for } \Theta = 0 \text{ and } \Theta = \pi/2 \qquad (10)$$

$$\frac{\partial \psi}{\partial r} + \frac{1}{2a} = 0 \qquad \text{for } r = a \qquad (11)$$

$$\frac{\partial \psi}{\partial r} + \frac{1}{R} (\psi - 1) = 0 \qquad \text{for } r = R. \qquad (12)$$

Having specified the boundaries of the region of interest, we then choose the grid layout. For simplicity, the spacing of grid points is chosen to be regular in both radial and angular variables. The radial coordinate is measured in units of a, and points are located from $(r/a) = 1$ to $(r/a) = R/a = 40$ in steps of 0.2. The value of the angular variable ranges from Θ to 0 to $\Theta = \pi/2$ in steps of $\pi/18$ (10°).

Since an iteration method is used to calculate ψ at each grid point, a trial solution is required to get started. For a run with momentum parameter P, a crude estimate of the energy is $E = (P^2 + 4a^2)^{1/2}$ [7]. Since the static solution with energy E is $\psi = 1 + E/2r$, we employ as the initial trial solution the function

$$\psi_0(r, \Theta) = 1 + (P^2 + 4)^{1/2}/2r.$$

where both P and r are measured in units of a.

It remains to transform the differential system (9)–(12) to finite differenced expressions for the matrix of grid values ψ_{ij}. Equation (9) is approximated by a standard second-order centered finite difference scheme. This non-linear relation then applies to all interior grid points. Rather than using the boundary conditions (10), the angular symmetries that led to them are employed directly by symmetrically extending the solution across the boundary and inserting the known values in the finite difference form of (9). Finally, the derivatives in boundary conditions (11) and (12) are approximated by a fourth-order difference scheme. Since these last conditions are linear, they may be solved algebraically for ψ on the radial boundaries.

With a system of difference equations for the ψ_{ij}'s in hand, we turn to the iterative calculation. The iterative method employed is successive over-relaxation (SOR) [9], which is the most efficient method known and is now used by all codes that solve the elliptic equations arising from Einstein's equations of general relativity [10]. The entire grid is swept out updating ψ_{ij} values point-by-point. At each grid point in the interior, the neighboring values of ψ_{ij} that are involved in the finite-difference form of Eq. (9) are momentarily fixed. The value of ψ_{ij} is then adjusted until it satisfies the still non-linear relation obtained from (9). This non-linear algebraic equation is

solved using Newton's method in an inner loop. Finally, the solution $\tilde{\psi}_{ij}$ from the inner loop is used to immediately update the value of ψ_{ij} by "overrelaxing":

$$\psi_{\text{new}} = \omega\tilde{\psi} + (1 - \omega)\,\psi_{\text{old}}.$$

Here ω is the over-relaxation or acceleration parameter which is adjusted to maximize convergence. For points on the radial boundaries, however, the (linear) boundary conditions are solved directly and applied immediately. The values on the boundary are *not* over-relaxed.

To test the convergence and stability properties of the iteration method, the model Hamiltonian, Eq. (6), is used in the non-linear term of (9). When the numerical solution and the known exact solution, Eq. (7), are compared for a broad range of the momentum P, one finds that several hundred iterations are sufficient for agreement to 0.1% or better at all points. Thus one may be confident that the numerical solution obtained for the real physical source (Eq. (5)) is a very good approximation to the actual factor satisfying (9).

3. DATA REDUCTION

In order to display the conformal factor from the data obtained by the iteration procedure, we must use symmetry conditions to continue the ψ function into the regions $r < a$ and $\pi/2 < \Theta < 2\pi$. (The azimuthal dimension continues to be suppressed.) For the radial extrapolation, we use the symmetry property of the conformal factor, Eq. (4),

$$\psi(r, \Theta) = (a/r)\,\psi(a^2/r, \Theta). \tag{13}$$

When we apply this symmetry to the numerical solution at radial grid points with $r \geqslant a$, we obtain by inversion the solution for interior points with $r < a$. Extrapolation to $r = 0.1a$ is sufficient for a good graphics display. Since Eq. (13) involves a non-linear map, we note that the interior radial grid points are no longer evenly spaced.

Although the global features of the conformal factor are apparent from a direct display, some of the fine points are not. To reveal certain subtleties of the solution, further data reduction is necessary. Two particular processes were utilized in this problem, each of which required forming ratios. To exhibit the radial dependence, the well-known conformal factor for a stationary black hole was divided by the iterated solution for a moving hole of the same total energy. In order to mask the strong radial dependence and reveal details of the angular dependence, the ratio of the conformal factor to its value along the line of motion ($\psi(r, \Theta)/\psi(r, 0)$) was formed.

To display the conformal factor and the divided data just described, I used the Program ASPEX [11]. Originally develped to generate maps of various geographic data, ASPEX can be used quite generally to plot functions of two variables. To use it, one must enter data in a rectangular matrix, in which the entries represent function

values at regular intervals. Various options for grid size, viewing angles, and vertical scaling may then be selected for display purposes.

Since my calculations produced ψ-values at regular intervals in polar coordinates, I had to recast my data into a rectangular $(z-x)$ grid. A simple four-point linear interpolation to a relatively small square grid with spacing $0.1a$ turned out to provide sufficiently accurate graphic displays. The interpolation was performed only in the first quadrant, since only there were original data and divided data available. Recall, however, that ψ depends on angle only through $\cos^2 \Theta$, a reflection symmetry. Thus the interpolated data were merely reflected through the x- and z-axes into the other quadrants.

The value at the origin presents a problem. ASPEX cannot simply leave out the origin (or any other point in the grid) when plotting; nor can it show ψ's true infinity there. This problem was solved by requiring that $\psi(z = 0, x = 0) = \psi(z = 0.1, x = 0)$. Thus, although the interpolated data are physically inaccurate right at the origin, the displays are continuous.

4. GRAPHIC DISPLAYS

The results of the numerical calculation are displayed in three different ways in order to highlight the various aspects of the solution. All use Eq. (8) for H as the source with $P = 10$ chosen as a typical momentum. These results appear in Figs. 2, 3, and 4.

Figure 2 shows the conformal factor ψ as a function of position in the region near the origin. As one might expect, ψ depends strongly on the radial distance, and diverges at the origin. It is also clear that the strong angular dependence in the source function H (see Fig. 1) is almost completely absent in the scale factor ψ. In fact, from Fig. 2 alone, the solution appears to be isotropic and indistinguishable from $\psi_{\text{Schwarz}} = 1 + E/2r$, the conformal factor for a static Schwarzschild black hole of rest energy E.

When we examine Fig. 3, the difference between ψ and ψ_{Schwarz} is in fact quite apparent. The figure shows the ratio $\psi_{\text{Schwarz}}/\psi$, where the E used in the Schwarzschild conformal factor is simply the total energy of the *moving* hole. (This energy is obtained from the surface integral $E = -(1/2\pi) \oint \nabla\psi \cdot d\mathbf{S}$ performed numerically at the outer boundary.) Thus Fig. 3 compares a moving black hole with a Schwarzschild hole of the same energy.

Figure 3 makes it clear that the radial dependence of ψ is in fact quite different from the conformal factor of a static hole. While they both approach 1 at large distances, ψ increases more slowly as the origin is approached. This can be understood when one looks directly at the differential equation (9), and assumes that any contribution to the Laplacian is almost entirely due to radial variation. If ψ behaves like $1 + Ar^n$ near the origin, then $\nabla^2\psi = (n + 1)(n) Ar^{n-2}$ so that $n > -1$ is needed for $\nabla^2\psi$ to be negative as required in Eq. (9). Thus ψ cannot increase as fast
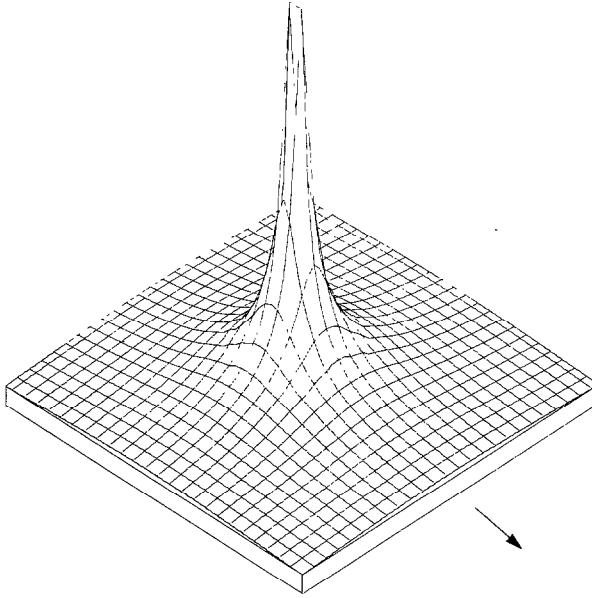
JEFFREY M. BOWEN

FIG. 2.   The conformal factor ψ, solution of Eq. (9), for $(P/a) = 10$. The plot shows a square region of side $5a$ centered on the origin. The value of ψ on this plot ranges from 1.75 at the corners to 13.9 near the center. Grid lines are drawn at intervals of $0.2a$, parallel to the z- and x-axes. The positive z direction (the direction in which the black hole is moving) is indicated by an arrow.
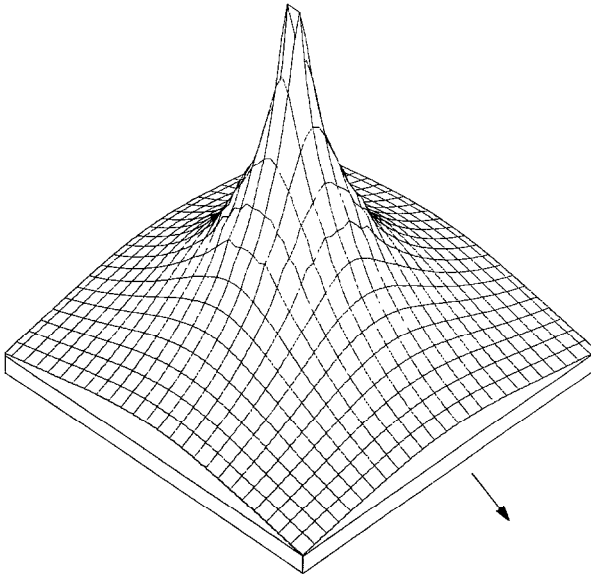

FIG. 3.   The ratio $\psi_{\text{Schwarz}}/\psi$ for $(P/a) = 10$. The plot shows the same square domain as in Fig. 2. Here the value of the ratio ranges from 1.46 at the edges to 4.10 near the center. The positive z-direction is indicated with an arrow.
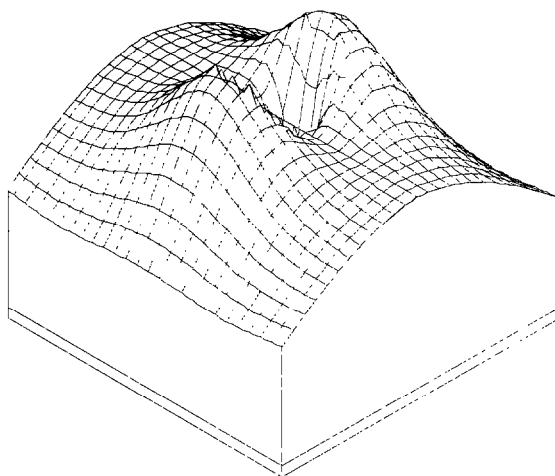
FIG. 4. The ratio $\psi(r, \Theta)/\psi(r, \Theta = 0)$ for $(P/a) = 10$. The plot shows the same square domain as in Fig. 2. The vertical scale is greatly exaggerated as the range of this ratio is only from 0.9886 to 1.0042. The minimum values of the ratio occur in two deep valleys which are symmetrically located between the hills on either side of the center reference line, the z axis.

as $1 + E/2r$ as the origin is approached. However, this effect is virtually impossible to detect from the display of undivided data, Fig. 2.

Finally, let us turn our attention to Fig. 4, which shows the ratio $\psi(r, \Theta)/\psi(r, \Theta = 0)$. In this plot we factor out the radial dependence and focus on the angular variations of the conformal factor. Since we have set **P** along the z-axis and also measure Θ from this direction, the value of ψ along the z-axis is chosen as the reference. The most striking feature is that $\partial\psi/\partial\Theta$ changes sign twice along any radial line (except the x- and z-axes, where $\partial\psi/\partial\Theta$ is zero by construction). Near $r = a$, ψ is maximum at $\Theta = 90°$, but at about $r = 1.8a$, the curve turns over and ψ $(\Theta = 0°)$ becomes the maximum. Since angular variation is not affected by the inversion map, we find that the curve turns over again at about $r = a^2/(1.8a) \approx 0.55a$, in between the hills of Fig. 4. Thus, there are two circles ($r \sim 1.8a$ and $r \approx 0.55a$) on which ψ is approximately constant. This effect went completely unnoticed [12] until displays like Fig. 4 were in hand.

5. Conclusions

The work reported here, in addition to its intrinsic value as the solution of an important problem in gravitational physics, presents three significant findings in the application of numerical methods and computer graphics to physical problems. The first is that the general method of successive over-relaxation (SOR) can easily be adapted to non-linear elliptic equations with unusual boundary or symmetry conditions. To make a problem suitable for an iterative calculation, a Dirichlet

condition at infinity can often be replaced with a Robin condition at a large but finite distance, such as Eq. (8). The inner boundary condition for this problem, Eq. (2), is an unusual mixed condition (not a Robin condition since the unit normal points into instead of out of the volume of integration) that nonetheless can be rewritten to express the boundary values in terms of those in the interior. Finally, certain symmetries can often be employed directly in the finite-differenced form of the elliptic operator, as was done for the reflection symmetries here, and thus eliminate extra boundary conditions. The tests with H_{model} show SOR to be a fast, efficient, and accurate method for these problems.

The second important finding is that physicists at small colleges or universities, who have limited knowledge of or access to sophisticated graphics software, can still produce perpective displays that are valuable guides in research. The ASPEX program at Bucknell runs on a Honeywell DPS/CP6, but it is compatible with any system that supports FORTRAN, has minimal graphics capability (DRAW, MOVE, PAGE) and offers 128K memory or sufficient overlay ability. Programs that make perpective drawings in polar coordinates do not seem to be readily available. Although the ASPEX program was designed for another purpose, it and other Cartesian-based perspective drawing packages can be adapted readily to display results in black-hole physics, scattering or potential theory, and other problems in which polar coordinates are the most natural.

The third significant aspect of this work that may be applicable to other problems concerns the modification of the conformal factor before display. As mentioned in Section 4, certain features of a solution to a new problem remain hidden in a straight display. Averaging, comparing to known special cases (as in Fig. 3), and dividing out approximate symmetries (as in Fig. 4), are all valuable tools for revealing subtle features not previously apparent.

REFERENCES

1. L. SMARR AND J. W. YORK. JR., *Phys. Rev. D* 17 (1978), 2529.
2. L. SMARR AND J. W. YORK, JR., *Phys. Rev. D* 17 (1978), 1945.
3. J. W. YORK, JR., Kinematics and dynamics of general relativity, *in* "Sources of Gravitational Radiation" (L. Smarr, Ed.), Cambridge Univ. Press, Cambridge, 1979.
4. C. W. MISNER, *Phys. Rev.* 118 (1960), 1110.
5. R. W. LINDQUIST, *J. Math. Phys.* 4 (1963), 938.
6. T. PIRAN AND J. W. YORK, JR., "Spacetime and Geometry, The Alfred Schild Lectures" (R. Matzner and L. Shepley, Eds.), pp. 147–176, Univ. of Texas Press, Austin, 1983.
7. J. M. BOWEN AND J. W. YORK, JR.. *Phys. Rev. D* 21 (1980), 2047.
8. J. M. BOWEN, Dissertation, University of North Carolina, Chapel Hill, 1979, unpublished.
9. See, for example. G. D. SMITH. "Numerical Solutions of Partial Differential Equations: Finite Difference Methods," pp. 227–268, Oxford Univ. Press, Oxford, 1978.
10. For a more complete discussion and further references, see Larry Smarr, *in* "Sources of Gravitational Radiation," p. 155, Cambridge Univ. Press, 1979.
11. ASPEX program developed by the Laboratory of Computer Graphics and Spatial Analysis, Graduate School of Design, Harvard University, MA, 1980.
12. T. PIRAN, private communication.